Nonlocal magnetoplasmons for cylindrical nanotubes in a perpendicular magnetic field

2004 J. Phys.: Condens. Matter 16 L389

(http://iopscience.iop.org/0953-8984/16/32/L03)

INSTITUTE OF PHYSICS PUBLISHING JOURNAL OF PHYSICS: CONDENSED MATTER

J. Phys.: Condens. Matter **16** (2004) L389–L394 PII: S0953-8984(04)79907-5

LETTER TO THE EDITOR

Nonlocal magnetoplasmons for cylindrical nanotubes in a perpendicular magnetic field

Godfrey Gumbs[1], **Chwen-Yang Shew**[2] **and M P A Fisher**[3]

[1] Department of Physics and Astronomy, Hunter College of the City University of New York, 695 Park Avenue, New York, NY 10021, USA
[2] Department of Chemistry, College of Staten Island of the City University of New York, 2800 Victory Boulevard, Staten Island, NY 10314, USA
[3] Institute for Theoretical Physics, Kohn Hall, 2315, University of California, Santa Barbara, CA 93106, USA

Received 26 April 2004
Published 30 July 2004
Online at stacks.iop.org/JPhysCM/16/L389
doi:10.1088/0953-8984/16/32/L03

Abstract

In this study, we report calculations of the collective plasmon excitations for an electron gas confined to the surface of a cylindrical nanotube in a magnetic field which is perpendicular to the axis of the cylinder. The eigenenergies of the single-particle states are first calculated. In a weak magnetic field, only a few of the lowest eigenstates show a coupling between the linear momentum along the axis of the nanotube and the angular momentum around its axis. Numerical results demonstrating this effect for various magnetic field strengths are presented. We then employ the random phase approximation (RPA) to obtain the density fluctuations due to a weak external perturbation by using the single-particle eigenstates to calculate the polarization function in the dispersion equation. Numerical results for the magnetoplasmon dispersion are presented for various magnetic field strengths.

In recent years, there has been a considerable amount of interest from both an experimental and theoretical point of view in the electronic transport and optical properties of carbon nanotubes [1, 2]. Of particular importance have been the plasmon excitations which have been studied for single-walled and multi-walled nanotubes, a linear array of nanotubes and the effects which an external magnetic field has on the plasmon excitations [3–18]. As far as we know, the applied magnetic field was along the axis of the nanotube [14, 15] and several interesting new effects were demonstrated including many cusps in the plasmon spectrum as a function of the magnetic flux through the tubule. The flux-dependent plasmon frequency has been shown to be proportional to the induced persistent-current density in the tubule [14, 15].

Our motivation for carrying out the present calculations is due to the fact that we may get a clearer understanding of the transport properties of systems of reduced dimensionality

by studying the plasmon excitation spectrum [19]. This is so because quasiparticles (magnetoplasmons here) determine the resistivity, as can be seen from the Kubo formula [20]. The role played by external fields in modifying the plasmon excitations of low-dimensional structures has been of particular interest [4, 5]. Several authors have investigated the response of nanotubes of various radii, which is relevant in considerations of the crossover from one dimensionality to another [6, 7, 9].

In this letter, we consider plasmon excitations in single-walled nanotubes using the RPA. We use a simple model to describe the electronic properties of the nanotubes. In our model, we assume that the electron system in a single cylindrical tubule consists of quasi-free electrons confined to the surface of an infinitely long cylinder of radius R. The tubule is embedded in a medium with dielectric constant ϵ_b. Based on this model, Lin and Shung [13] calculated the plasmon spectrum in a single cylindrical tubule and in a system of several co-axial cylindrical tubules. Gumbs and Ǎizin [10] recently obtained the plasmon excitations for a linear array of nanotubes consisting of an arbitrary number of tubules in the absence of an external magnetic field. We first calculate the single-particle energy eigenstates for these electrons in the presence of a magnetic field applied in a direction perpendicular to the axis of the nanotube. The energy eigenvalues are analysed as functions of magnetic field and momentum along its axis by solving numerically the Schrödinger equation in a magnetic potential. We introduce the Coulomb interaction between electrons and determine the charge density fluctuations due to a weak external field. We use RPA to obtain the magnetoplasmon dispersion equation and numerical results are presented. Specifically, we develop a general formulation which can be used to derive the dispersion equation for magnetoplasmons for an arbitrary number of concentric tubules when a magnetic field is applied perpendicular to the axis of the nanotube. What makes this different from the case of a parallel magnetic field is that the magnetic field couples the linear motion along the axis of the nanotube with the orbital motion around the axis, i.e., the eigenstates cannot be labelled by the angular momentum quantum number because of mode coupling. This leads to some features in the plasmon excitation spectrum which become more pronounced with increasing magnetic field.

Consider an electron with effective mass m^* confined on the surface of a circular cylinder of radius R, in the presence of a uniform magnetic field B (parallel to the y axis) perpendicular to its axis, taken to be the z direction. We use the gauge $A_x = 0$, $A_y = 0$, $A_z = -BR\cos\varphi$, where φ is the angle the radius vector makes with the positive x axis. It is a simple matter to show that the eigenfunctions are

$$\psi_\alpha(r,\varphi,z) = \frac{1}{\sqrt{L_z}} e^{ik_z z}\Phi(r)\Psi_l(\varphi), \qquad \Phi^2(r) = \delta(r-R), \tag{1}$$

where Ψ_l is a solution of the Schrödinger equation

$$-\frac{\hbar^2}{2m^*R^2}\frac{d^2\Psi(\varphi)}{d\varphi^2} + V_{\text{eff}}(\varphi)\Psi(\varphi) = \tilde{\epsilon}\Psi(\varphi) \tag{2}$$

in the presence of the magnetic potential given by

$$V_{\text{eff}}(\varphi) \equiv \frac{e\hbar k_z BR}{m^*}\cos\varphi + \frac{e^2B^2R^2}{2m^*}\cos^2\varphi. \tag{3}$$

The energy eigenvalues are

$$\epsilon_\alpha = \frac{\hbar^2k_z^2}{2m^*} + \tilde{\epsilon}_l(k_z), \tag{4}$$

with $\alpha = \{k_z, l\}$, $k_z = \dfrac{2\pi n}{L_z}$ and $n = 0, \pm1, \pm2, \ldots$. The subscript '$l$' labels the eigenstates for a chosen value of k_z. We have solved equation (2) numerically for the 'Landau levels'

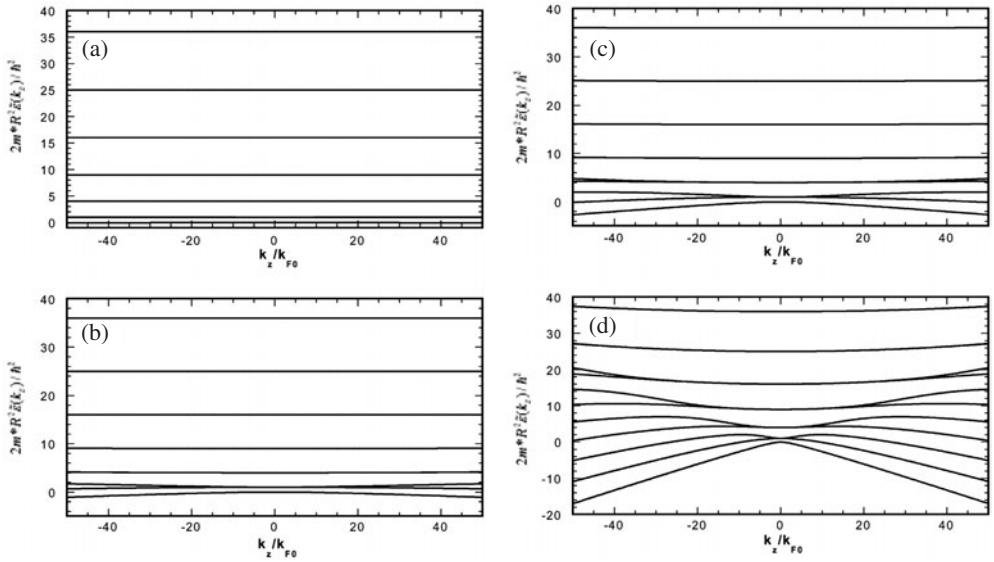

Figure 1. Calculated energy eigenvalues $\tilde{\epsilon}$ (scaled by $\hbar^2/2m^*R^2$) of the Schrödinger equation (2) as a function of the wavevector k_z/k_{F0}. Here, k_{F0} is the Fermi wavenumber in the ground ($l = 0$) subband in the absence of magnetic field. The parameters used in the calculation are $m^* = 0.25\,m_e$ where m_e is the bare electron mass and $R = 11.0$ Å. The magnetic fields B chosen are (a) 1 T, (b) 5 T, (c) 10 T and (d) 50 T.

of a tubule and our results are plotted in figure 1 for various magnetic field strengths. The energy eigenvalues $\tilde{\epsilon}_l(k_z)$ in equation (4) depend on k_z due to the coupling between the angular momentum around the axis of the tubule with the linear momentum parallel to its axis [21]. This coupling is strongest for the lower energy levels (low angular momentum).

The energy eigenvalues are not equally spaced in general but the separation between adjacent levels is approximately $\hbar\omega_c$ for the higher energy levels in a high magnetic field, where ω_c is the cyclotron frequency. To better understand the effects due to a perpendicular magnetic field on the electronic states, the energy eigenvalues were calculated numerically, and our results are presented in figures 1(a)–(d). Here, we plot the quantized energy levels $\tilde{\epsilon}_l(k_z)$ as a function of k_z for several magnetic fields. In figure 1(a), all the energy eigenvalues are almost independent of k_z due to a weak coupling between the linear motion parallel to and the angular momentum around the axis of the tubule at low magnetic fields. As the magnetic field is increased in figures 1(b) through (d), Landau levels appear for the lower energy eigenvalues. In fact, the separation between adjacent levels is approximately $\hbar\omega_c$ for the higher energy levels in a high magnetic field such as figure 1(d), where $\omega_c = eB/m^*$ is the cyclotron frequency. Also, these energy levels exhibit a stronger dependence on wavenumber for larger $|k_z|$. The Landau level separation in high magnetic fields for $k_z \approx 0$ can be deduced from equation (3) by neglecting the first term of $V_{\rm eff}(\varphi)$ and then using a harmonic approximation at small angle for $\cos^2\varphi$.

It may be shown in the RPA that the magnetoplasmon excitations can be obtained from the following determinantal form of the dispersion equation:

$$\mathrm{Det}\left[\delta_{LL'} + \frac{e^2}{\pi\varepsilon_s} I_L(q_z R) K_L(q_z R)\chi_{LL'}(q_z,\omega)\right] = 0, \tag{5}$$

where $\varepsilon_s = 4\pi\epsilon_0\epsilon_b$ and $I_L(x)$ and $K_L(x)$ are modified Bessel functions of the first and second

kind, respectively. Also,

$$\chi_{LL'}(q_z,\omega) = \sum_{l,l'=-\infty}^{\infty} M^*_{l,l'}(L) M_{l,l'}(L') \Pi_{ll'}(q_z,\omega) \tag{6}$$

is the susceptibility for a tubule of radius R, $L = 0, \pm 1, \pm 2, \ldots$, and the polarization function is

$$\Pi_{ll'}(q_z,\omega) = 2\int_{-\infty}^{\infty} \mathrm{d}k_z \, \frac{f_0(\epsilon_{k_z l}) - f_0(\epsilon_{k_z - q_z, l'})}{\hbar\omega + \epsilon_{k_z - q_z, l'} - \epsilon_{k_z l}}, \tag{7}$$

with $f_0(\epsilon)$ the Fermi function, and we have introduced the form factor

$$M_{l,l'}(L) \equiv \int_0^{2\pi} \mathrm{d}\varphi \; \Psi^*_l(\varphi) \Psi_{l'}(\varphi) \mathrm{e}^{\mathrm{i}L\varphi}. \tag{8}$$

The k_z-integral in equation (7) cannot be carried out analytically even at $T = 0$ K using the energy eigenvalues in equation (4) because of the dependence of $\tilde{\epsilon}_l(k_z)$ on the wavevector when there is a finite perpendicular magnetic field present[4]. However, in the absence of an external magnetic field, $\Psi_l(\varphi) = \frac{1}{\sqrt{2\pi}} \mathrm{e}^{\mathrm{i}l\varphi}$ where $l = 0, \pm 1, \pm 2, \ldots$ and $M_{l,l'}(L) = \delta_{l',l-L}$, which makes the matrix in equation (6) diagonal in (L, L'), i.e., angular momenta are decoupled so that the plasmon excitations may be labelled by the angular momentum transfer (in units of $\hbar$) $L = l - l'$. As a matter of fact, equation (5) agrees with the dispersion formula in Lin's paper [13] in zero external magnetic field, i.e., $\epsilon(q_z, L, \omega) = 0$ where $\epsilon(q_z, L, \omega)$ denotes the diagonal elements in equation (5).

We now present and discuss our numerical results for the dispersion relation of the magnetoplasmons. To closely simulate the graphene tubule, we took $\varepsilon_\mathrm{b} = 2.4$, $m^* = 0.25\, m_\mathrm{e}$ where m_e is the bare electron mass, $R = 11.0$ Å and $E_\mathrm{F} = 0.6$ eV. The effective Bohr radius is $a_\mathrm{B} \equiv \hbar^2 \varepsilon_\mathrm{s}/m^* e^2 = 5.08$ Å. All calculations were carried out at zero temperature. We included the transitions $L = 0$ only in these calculations so that we have a scalar for equation (5). For these chosen values of the parameters, there are only five subbands occupied by electrons corresponding to $l = 0, \pm 1, \pm 2$ in the absence of an external magnetic field. There are three quasi-acoustic plasmon branches associated with intra-subband electron excitations with angular momentum transfer $L = 0$. We have solved equation (5) for various values of external magnetic field and present our results in figure 2. We used these values for the radius of the tubule, the background dielectric constant and electron effective mass to compare with the zero-field case which was presented by Lin and Shung [14]. It was shown that there are three acoustic plasmon modes in the absence of magnetic field and they lie in the pockets of the particle-hole modes (see figure 2 of [13].) Also, we note that the carbon nanotube we are modelling is semiconducting so that the energy dispersion is quadratic at the top of the valence band and at the bottom of the conduction band [22]. This is in contrast to metallic tubules for which the corresponding energy band is linear in wavevector.

For the magnetic field chosen in figure 2(a), we have $\hbar\omega_\mathrm{c}/E_\mathrm{F} \approx 0.135$. The splitting of the highest plasmon branch in figure 2(a) is higher than the cyclotron frequency and is very interesting. As the magnetic field is increased, Landau levels are formed, and some of these Landau levels lie close to the Fermi level. The value of the wavevector where the Landau levels cross the Fermi level decreases with increasing magnetic field. The splitting of the highest plasmon branch is due to inter-Landau level transitions near the Fermi level, and the wavevector

[4] We note that in high magnetic fields, some of the energy bands below E_F may have negative energy dispersion as shown in figure 1(d). In calculating the polarization function in equation (7) at $T = 0$ K, there is no cut-off wavevector for these bands. However, because the energy enters the polarization function in the denominator, there is convergence of the numerical result when the integration range is sufficiently large.

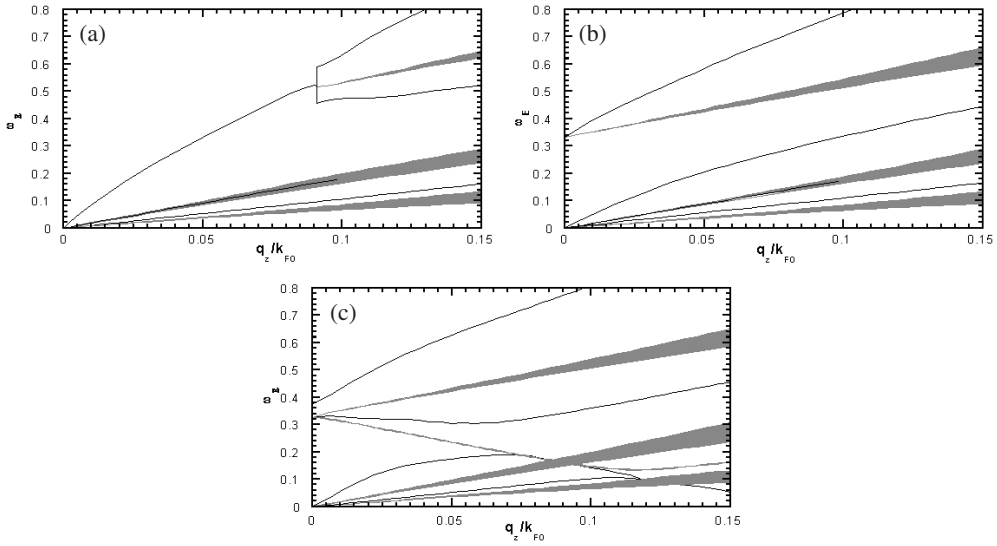

Figure 2. The intra-subband magnetoplasmons ($L = 0$), shown as solid curves, in the presence of an applied magnetic field. For the magnetic field chosen, we have $\hbar\omega_c/E_F \approx 0.135$ in (a), 0.145 in (b), and 0.15 in (c) where ω_c is the cyclotron frequency. The plasmon excitation energy, in units of the Fermi energy ω_F, is plotted as a function of q_z, in units of the Fermi wavenumber k_{F0} in the ground ($l = 0$) subband. The results were obtained by solving equation (5). The parameters used in the calculation are $\varepsilon_b = 2.4$, $m^* = 0.25\ m_e$ where m_e is the bare electron mass and $R = 11$ Å, $E_F = 0.6$ eV. Shaded regions correspond to the particle-hole mode continuum.

at which this splitting occurs is consequently reduced as the magnetic field is increased. Figure 2(a) shows that the highest quasi-acoustic plasmon branch starts to split at $q_z \approx 0.09k_{F0}$, where k_{F0} is the Fermi wavevector for the subband with angular momentum quantum number $l = 0$. For $q_z \gtrsim 0.09k_{F0}$, the splitting also induces the formation of an additional particle-hole mode region due to the single-particle transitions between Landau levels. This particle-hole mode region is located between the two split plasmon modes. Furthermore, as the magnetic field is increased, the wavevector at which the splitting of the highest mode occurs decreases. In addition, the frequency of the lower branch of these two split modes tends to zero as B increases. We illustrate this in figure 2(b), which shows that the splitting occurs close to $q_z = 0$ as the magnetic field is increased so that $\hbar\omega_c/E_F \approx 0.145$. The highest magnetoplasmon mode and the additional particle-hole mode region display similar behaviour near $\hbar\omega/E_F \equiv \omega_E = 0.33$ at a wavevector near $q_z = 0$. However, the magnetoplasmon mode below the additional particle-hole mode region falls to $\omega_E \approx 0$ at $q_z = 0$. The magnetoplasmon and particle-hole modes which lie below this region of excitations all have zero frequency in the long wavelength limit.

Figure 2(c) shows that as the magnetic field is increased so that $\hbar\omega_c/E_F \approx 0.15$, the excitation spectrum displays an even more complicated pattern. The magnetoplasmon spectrum has branches which split off from the particle-hole mode region at finite wavevector. These branches are due to inter-subband transitions between Landau levels. The results in figure 1 show that as the magnetic field is increased, Landau levels may cross the Fermi level. The number of these branches depends on the magnetic field because how many subbands lie below E_F is a function of magnetic field. We have observed similar features for larger cylinder radii (data not shown) at lower magnetic fields, because the cylinder radius determines the subband occupation for a chosen Fermi level, and this number increases with the radius R.

Figure 2(c) also shows that in high magnetic field, some of the plasmon excitations have negative group velocity for a range of values of the wavevector along the axis of the tubule. The Coulomb interaction separates a collective excitation above and another below the particle-hole region due to intra- and inter-subband transitions. The negative dispersion arises from anticrossing of these two branches of magnetoplasmons. The results we derived demonstrate that the coupling between the fluctuations along the axis of the tubule and the orbital motion around the axis results in a shift in the dispersion curve from the particle-hole spectrum which strongly depends on magnetic field. Also, the oscillator strengths of the magnetoplasmons are functions of the magnetic field but the highest branch is likely to have largest weight [13].

The dispersion equation we derived was based on the RPA, and the numerical results we presented were for intra-subband transitions ($L = 0$) only. If correlation effects are included beyond the RPA, the qualitative nature of the obtained results should not change because the density we chose is low. Also, our conclusions should not be affected for inter-subband transitions corresponding to $L \neq 0$.

We acknowledge partial support from the National Science Foundation under grant No PHY99-07949 and a CUNY Collaborative Incentive Award No 80209-08-08. GG received support in part from PSC-CUNY grant No 64513-00-33 as well as grant No 4137308-04 from the NIH. CYS is grateful for the support from PSC-CUNY grants Nos 64379-00-33, 65367-00-34 and 66409-00-35.

References

[1] Lin-Chung P J and Rajagopal A K 2002 *Phys. Rev.* B **65** 113408
[2] See, for example, Bertsch G F and Broglia R A 1994 *Oscillations in Finite Quantum Systems* (New York: Cambridge University Press)
[3] Que W 2002 *J. Phys.: Condens. Matter* **14** 5239
[4] Bertsch G F, Bulgac A, Tománek D and Wang Y 1991 *Phys. Rev. Lett.* **67** 2690
[5] Alasia F *et al* 1994 *J. Phys. B: At. Mol. Opt. Phys.* **27** L643
[6] Broglia R A, Alasia F, Arcagni P, Colo G, Ghielmetti F, Milani C and Roman H E 1997 *Z. Phys.* D **40** 240
[7] Yabana K and Bertsch G F 1997 *Z. Phys.* D **42** 219
[8] Vasvári B 1997 *Phys. Rev.* B **55** 7993
[9] Bianchetti M, Buonsante P F, Ginelli F, Roman H E, Broglia R A and Alasia F 2002 *Phys. Rep.* **357** 459
[10] Gumbs G and Aĭzin G R 2002 *Phys. Rev.* B **65** 195407
[11] Gumbs G 2002 *Phys. Rev.* B **66** 205413
[12] Gumbs G and Balassis A 2003 *Phys. Rev.* B **68** 075405
[13] Lin M F and Shung K W-K 1993 *Phys. Rev.* B **47** 6617
[14] Lin M F and Shung K W K 1993 *Phys. Rev.* B **48** 5567
[15] Lin M F and Shung K W-K 1995 *Phys. Rev.* B **52** 8423
[16] Lin-Chung P J and Rajagopal A K 1994 *Phys. Rev.* B **49** 8454
[17] Lin M F and Chuu D S 1998 *Phys. Rev.* B **57** 10183
[18] Lin M F, Shyu F L and Chen R B 2000 *Phys. Rev.* B **61** 14114
[19] See, for example, Bertsch G F and Broglia R A 1994 *Oscillations in Finite Quantum Systems* (New York: Cambridge University Press)
[20] Baranger H and Stone A D 1989 *Phys. Rev.* B **40** 8169
[21] Ajiki H and Ando T 1993 *J. Phys. Soc. Japan* **62** 1255
[22] Saito R, Dresselhaus G and Dresselhaus M S 1998 *Physical Properties of Carbon Nanotubes* (London: Imperial College Press) p 110